# Configuration mixing and relative transition rates between low-spin states in $^{68}$Ni

F. Recchia,[1,*] C. J. Chiara,[2,3] R. V. F. Janssens,[3] D. Weisshaar,[1] A. Gade,[1,4] W. B. Walters,[2] M. Albers,[3] M. Alcorta,[3]
V. M. Bader,[1,4] T. Baugher,[1,4] D. Bazin,[1] J. S. Berryman,[1] P. F. Bertone,[3,†] B. A. Brown,[1,4] C. M. Campbell,[5]
M. P. Carpenter,[3] J. Chen,[6] H. L. Crawford,[5] H. M. David,[3,7] D. T. Doherty,[3,7] C. R. Hoffman,[3] F. G. Kondev,[6] A. Korichi,[3,8]
C. Langer,[1] N. Larson,[1,9] T. Lauritsen,[3] S. N. Liddick,[1,9] E. Lunderberg,[1,4] A. O. Macchiavelli,[5] S. Noji,[1] C. Prokop,[1,9]
A. M. Rogers,[3,‡] D. Seweryniak,[3] S. R. Stroberg,[1,4] S. Suchyta,[1,9] S. Williams,[1] K. Wimmer,[1,10] and S. Zhu[3]

[1]*National Superconducting Cyclotron Laboratory, Michigan State University, East Lansing, Michigan 48824, USA*
[2]*Department of Chemistry and Biochemistry, University of Maryland, College Park, Maryland 20742, USA*
[3]*Physics Division, Argonne National Laboratory, Argonne, Illinois 60439, USA*
[4]*Department of Physics and Astronomy, Michigan State University, East Lansing, Michigan 48824, USA*
[5]*Nuclear Science Division, Lawrence Berkeley National Laboratory, Berkeley, California 94720, USA*
[6]*Nuclear Engineering Division, Argonne National Laboratory, Argonne, Illinois 60439, USA*
[7]*School of Physics and Astronomy, University of Edinburgh, Edinburgh EH9 3JZ, United Kingdom*
[8]*CSNSM-IN2P3/CNRS, F-91405 Orsay Campus, France*
[9]*Department of Chemistry, Michigan State University, East Lansing, Michigan 48824, USA*
[10]*Department of Physics, Central Michigan University, Mt. Pleasant, Michigan 48859, USA*

The low-spin level scheme of $^{68}$Ni was investigated following two-neutron-knockout and multinucleon-transfer reactions. The energy of the first excited state was determined to be $E_x(0_2^+) = 1603.5(3)$ keV. Relative $B(E2)$ transition probabilities were deduced and compared with shell-model calculations using several modern effective interactions. Theory reproduces the data well, but indicates substantial mixing of multi-particle, multi-hole configurations for the lowest observed $0^+$ and $2^+$ states.

PACS number(s): 23.20.Lv, 21.10.Tg, 21.60.Cs, 27.50.+e

In atomic nuclei, the phenomenon of shape and configuration coexistence can emerge in the proximity of shell and subshell closures [1]. In even-even nuclei, this manifests itself as competition between low-lying $0^+$ states that differ in their particle-hole content. The nucleus $^{68}$Ni, with 28 protons (closed shell) and 40 neutrons (harmonic-oscillator shell gap separating the $fp$ and $g_{9/2}$ orbitals), is such a system where the low-energy structure is sensitively determined by the interplay and mixing of a variety of particle-hole excitations. In fact, three of its four lowest-energy levels have spin and parity $I^\pi = 0^+$ [2–5]. Given that the first excited state is the $0_2^+$ state, it can only decay by an isomeric $E0$ transition (half-life $t_{1/2} = 270(5)$ ns [6]) to the $0_1^+$ ground state, proceeding by either internal conversion or pair production.

For decades, the excitation energy $E_x = 1770(30)$ keV of the $0_2^+$ isomer, obtained by Bernas *et al.* [2] using particle-spectroscopy techniques with the $^{70}$Zn($^{14}$C,$^{16}$O) transfer reaction, was the only direct measurement for this state. Although the uncertainty was quoted as 30 keV, comparisons of early transfer-reaction data for $^{67,68}$Ni [2,7] with subsequent, higher-precision $\gamma$-ray studies (e.g., Refs. [3,8,9]) reveal a systematic ~100- to 200-keV offset in the excitation spectrum from which one may infer the $0_2^+$ isomer to be lower in

energy than reported. However, only recently did Suchyta *et al.* [10] directly measure the electrons produced in $E0$ decay following $^{68}$Co $\beta$ decay. These new data provided not only an improved value for the energy of the $0_2^+$ state [1605(3) keV], but also indicated the presence of prompt 1138- and 2420-keV transitions preceding the $E0$ decay [10].

In addition to the $0_1^+$ and $0_2^+$ states, a 2511-keV $0_3^+$ level was tentatively proposed following $\beta$ decay [4]. This assignment was later firmly established in a deep-inelastic-scattering (DIS) experiment [5]. Recently, a fourth, isomeric ($t_{1/2} = 216_{-50}^{+66}$ ns) $0^+$ state at 2202 keV was proposed [11]; however, no evidence for this state was found in another study despite the use of similar reactions [5].

As noted above, the presence of multiple low-energy $0^+$ states such as these is indicative of configuration or shape coexistence [1]. Monte Carlo shell-model (MCSM) calculations using an $fpg_{9/2}d_{5/2}$ model space [10,12,13] suggested that spherical, oblate, and prolate deformed minima coexist below 3 MeV in $^{68}$Ni, likely corresponding to the $0_1^+$, $0_2^+$, and $0_3^+$ states, respectively. Furthermore, the $2_1^+$ and $0_2^+$ levels were predicted to be members of the same oblate structure.[1]

Suchyta *et al.* [10] focused on the energy and $E0$ decay of the repositioned $0_2^+$ isomer and the implications for shape coexistence in $^{68}$Ni. In this Rapid Communication, we discuss the nature of the higher-spin states directly associated with the various $0^+$ states and the consequences for their

---

*Present address: Dipartimento di Fisica e Astronomia "Galileo Galilei", Università degli Studi di Padova, I-35131 Padova, Italy.

†Present address: Marshall Space Flight Center, Huntsville, Alabama 35812, USA.

‡Present address: Nuclear Science Division, Lawrence Berkeley National Laboratory, Berkeley, California 94720, USA.

---

[1]Note that shape coexistence has been proposed for the low-spin level structure of neutron-rich Cr and Fe isotopes [14].
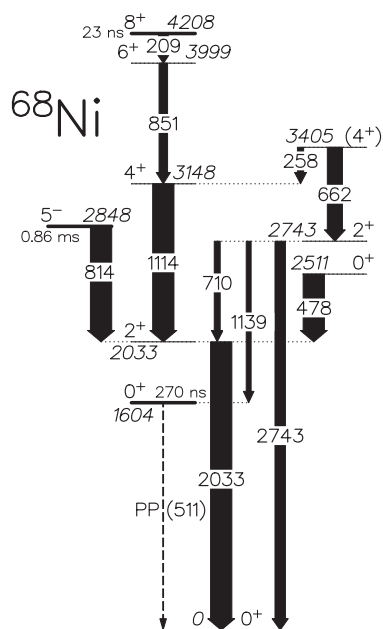
FIG. 1. Partial level scheme of $^{68}$Ni. Arrow widths are proportional to the branching ratios measured in the DIS data. Spins and parities are taken from Refs. [5,9,15,16] and half-lives from Refs. [15,16]. The dashed line marked PP(511) denotes the $E0$ decay by pair production (see text).

configurations. Results presented here originate from two in-beam spectroscopy experiments that complement the information obtained from decay spectroscopy [10] and provide a comprehensive picture of the low-lying level structure of $^{68}$Ni. The relevant details are summarized in the partial level scheme of Fig. 1. The decay patterns of several states are examined in terms of relative $B(E2)$ strengths, in order to investigate further the intrinsic structures involved. These results provide additional tests for modern shell-model calculations that also aim to describe exotic nuclei in the $fpg_{9/2}(d_{5/2})$ valence space.

Excited states in $^{68}$Ni were populated in two experiments involving different reaction mechanisms. At the ATLAS facility at Argonne National Laboratory, a 440-MeV $^{70}$Zn beam was directed onto a $^{208}$Pb target that was sufficiently thick to stop all reaction products in the center of the Gammasphere array of 100 Compton-suppressed high-purity germanium (HPGe) detectors [17]. Details of the experimental setup are provided in Ref. [5]. There are two key features relevant to the present discussion: (i) the time structure of the beam, with 0.3-ns beam pulses every 412 ns enabling prompt and delayed tagging of $\gamma$ rays, and (ii) the excitation of cross-coincident partner nuclei in the DIS process, specifically the population of Po isotopes with $A \leqslant 210$ for $^{68}$Ni.

$^{68}$Ni was also produced in two-neutron knockout (2nKO) reactions at the Coupled Cyclotron Facility of the National Superconducting Cyclotron Laboratory (NSCL). A secondary cocktail beam containing $^{70}$Ni, $^{69}$Co, and $^{71}$Cu ions was produced in the projectile fragmentation of a 140-MeV/u $^{82}$Se beam on a 423-mg/cm$^2$ $^9$Be production target located at the entrance of the A1900 fragment separator [18]. The momentum acceptance of the separator was set to 1%. Secondary beams with typical intensities of $10^5$ ions/s were delivered

to the experimental area and impinged upon a 281-mg/cm$^2$ $^9$Be reaction target located at the pivot point of the S800 spectrograph [19] to induce knockout reactions at a midtarget energy of 75 MeV/u. Reaction products were identified on an event-by-event basis at the S800 focal plane [19]. The high-resolution $\gamma$-ray detection system GRETINA [20,21], an array of 36-fold segmented HPGe detectors, surrounded the S800 target position and was used to detect prompt $\gamma$ rays emitted by the projectile-like reaction residues. The GRETINA quadruple-crystal detector modules were arranged in two rings, with four detectors located at 58° and three at 90° with respect to the beam axis. Signal decomposition [21] provided sub-segment spatial resolution used for the event-by-event Doppler reconstruction of the $\gamma$ rays emitted in flight by the projectile-like reaction products. The photopeak efficiency of the detector array was calibrated with standard sources and corrected for the Lorentz boost of the $\gamma$-ray distribution emitted by the recoils moving at velocity $0.38c$. Finally, delayed $\gamma$ rays could also be identified within a 0.4- to 25-$\mu$s time window following implantation of the ions in an Al plate in front of a $4 \times 8$ array of CsI(Na) detectors located behind the focal plane of the S800 spectrograph [22,23].

With the $\sim$50-ns flight time for $^{68}$Ni ions through the S800 spectrograph, it was possible to correlate isomeric decays measured using the CsI(Na) detectors with prompt $\gamma$ rays at the target position. Figure 2(a) presents the CsI(Na) spectrum measured in coincidence with $^{68}$Ni, 2nKO-reaction fragments wherein a 511-keV peak is observed. A 511-keV line is expected following decay of the $0_2^+$ isomer via pair production (PP). Gating on the 511-keV $\gamma$ ray in the CsI(Na) scintillators returns the coincidence spectrum of Fig. 2(b), revealing prompt 663(1)- and 1139(1)-keV transitions detected by GRETINA. The former had been identified in Ref. [5] as feeding the $2_2^+$ level at 2743 keV (see Fig. 1). A transition with the latter energy had been reported in the $\beta$-decay work of Ref. [4], but no coincidence relationships were observed. At the time, the large systematic offset in the $^{68}$Ni $0_2^+$ energy had not
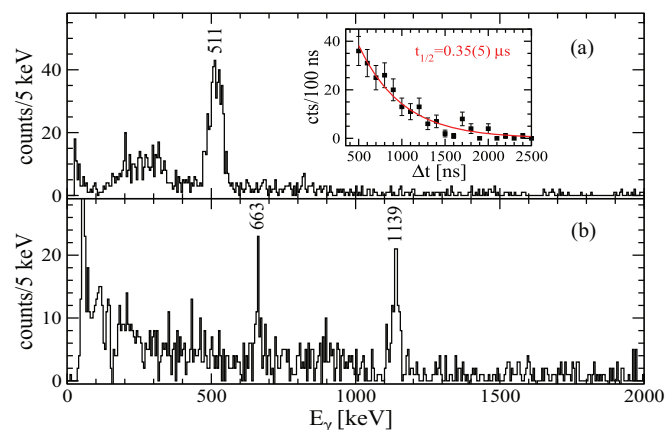


FIG. 2. (Color online) Spectra from the 2nKO data. (a) Delayed $\gamma$-ray spectrum recorded in the CsI(Na) scintillators in coincidence with implanted $^{68}$Ni ions. Inset: decay curve for the 511-keV line. (b) Prompt GRETINA spectrum coincident with the identification of a $^{68}$Ni recoil and the detection of a delayed 511-keV $\gamma$ ray in the CsI(Na) detectors.
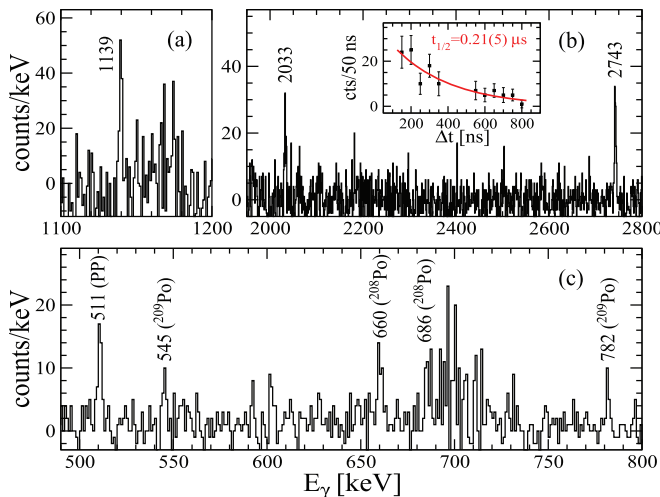
FIG. 3. (Color online) Spectra from the DIS data. (a), (b) Prompt $\gamma$ rays coincident with the 662-keV $\gamma$ ray and delayed $^{208,209}$Po lines. (c) Delayed $\gamma$ rays coincident with prompt 662- and 1139-keV transitions. Inset to (b): decay curve for the 511-keV line; random events associated with the next beam burst at ~400 ns are excluded from the fit.

been recognized, and Mueller *et al.* [4] proposed that the 1139-keV $\gamma$ ray likely feeds the long-lived $5^-$ isomer. The coincidence relationship between prompt 1139- and delayed 511-keV $\gamma$ rays observed in the present work, as well as the relative intensities of the 663- and 1139-keV lines, indicate that the latter should be placed above the $0_2^+$ isomer, likely depopulating the known 2743-keV, $2_2^+$ level and, thus, fixing the $0_2^+$ energy at 1604(1) keV, in agreement with Suchyta *et al.* [10].

This placement of the 1139-keV $\gamma$ ray is confirmed in the DIS data. Figures 3(a) and 3(b) provide a prompt coincidence spectrum produced by a double gate on the prompt 662.5-keV transition[2] in $^{68}$Ni and delayed $\gamma$ rays in the partner nuclei $^{208}$Po (660 and 686 keV [24]) and $^{209}$Po (782 and 545 keV [25]); a peak at 1139.2(3) keV is apparent. Double gating on the prompt 662- and 1139-keV transitions produces the spectrum of delayed $\gamma$ rays in Fig. 3(c), where the 511-keV annihilation line is present along with several Po lines. The observed coincidence relationships require that the 1139-keV $\gamma$ ray must directly feed the $0_2^+$ isomer. These data provide the most precise energy available thus far for the $0_2^+$ state: 1603.5(3) keV.

The placement described above is further supported by determination of the half-life of the 511-keV isomeric decay line in both measurements [Figs. 2(a) and 3(b) insets]. The measured $t_{1/2}$ values are reasonably consistent with the 0.270(5)-$\mu$s half-life reported for the $0_2^+$ state in Ref. [6].

In both data sets, the 2743-keV $2_2^+$ state has been observed to decay by three parallel paths: the 710-keV $M1/E2$ transition ($\delta = -1.5^{+0.9}_{-1.2}$ [5]) to the 2033-keV $2_1^+$ level, the new 1139-keV $E2$ $\gamma$ ray to the repositioned $0_2^+$ isomer, and the

---

[2]The energy 662 keV from the more precise Gammasphere data will be used in the subsequent discussion.

TABLE I. Intensities $I_\gamma$ and $B(E2)$ ratios $R(E_\gamma)$ (see text) for transitions from the $2_2^+$ state in $^{68}$Ni. The bottom row provides weighted averages of the values from the two data sets presented here (DIS and 2nKO) and the earlier $\beta$-decay work [4].

| Reaction | $I_\gamma(2743)$, $2_2^+ \to 0_1^+$ | $I_\gamma(1139)$, $2_2^+ \to 0_2^+$ | $I_\gamma(710)$, $2_2^+ \to 2_1^+$ | $R(1139)$ | $R(710)$ |
|---|---|---|---|---|---|
| DIS | 100(11) | 47(10) | 58(10) | 38(9) | $346^{+117}_{-225}$ |
| 2nKO | 100(3) | 50(6) | 52(9) | 41(5) | $310^{+100}_{-199}$ |
| $\beta$ [4] | 100(5) | 42(3) | 41(3) | 34(3) | $244^{+69}_{-152}$ |
| Average | 100(3) | 44(3) | 43(3) | 36(2) | $259^{+73}_{-161}$ |

2743-keV $E2$ transition directly to the ground state. The presence of several branches offers an opportunity to explore the nature of the $0^+$ and $2^+$ states further by examining the properties of these transitions. Although an absolute determination of the $B(E2)$ strengths would require knowledge of the half-life of the $2_2^+$ state, or a direct measurement of the $B(E2)$ value for one of the transitions, the *relative* strengths can be compared to those predicted by different calculations.

In the DIS data, the spectrum in Figs. 3(a) and 3(b) was used to determine the intensities of the 710-, 1139-, and 2743-keV $\gamma$ rays. The areas of the latter two peaks were measured directly. A fit of the 710-keV line was deemed unreliable because of the presence of contaminants in this part of the spectrum. Instead, as the full intensity of the 710-keV transition (as seen when gated from above) must also pass through the 2033-keV $\gamma$ ray, the area of the latter peak served as a surrogate. A correction for the $\gamma$-ray efficiencies yielded relative intensities; from these, the $B(E2)$ rates were expressed as ratios with respect to the 2743-keV $\gamma$ ray, given as $R(E_\gamma) = B(E2; E_\gamma, 2_2^+ \to I^+)/B(E2; 2743, 2_2^+ \to 0_1^+)$. The ratios obtained in this way are given in Table I. For the 710-keV transition, the mixing ratio deduced in Ref. [5] was used to determine the $E2$ component of the intensity.

A similar analysis was carried out for the 2nKO data, with the intensities of the three $\gamma$-ray branches, appropriately efficiency-corrected, determined from the singles spectrum measured with GRETINA. The measurement for the 710-keV line is complicated by the presence of a known 709-keV $(6^-) \to 5^-$ transition in $^{68}$Ni which cannot be readily resolved. The contribution from this contaminant can be determined, however, from the intensity of the 113-keV $\gamma$ ray depopulating the same $(6^-)$ state by using the previously measured $I_\gamma(709)/I_\gamma(113)$ branching ratio [16]. Similarly, an 1152-keV $6^+ \to 5^-$ transition interferes with the 1139-keV line; here, the contamination was quantified through the branching ratio with the measurable 851-keV transition [26]. In both cases, the contaminant accounts for about half of the peak and dominates the uncertainty for the intensity. The resulting $I_\gamma$ values and corresponding $B(E2)$ ratios from the 2nKO data are included in Table I.

Finally, although the 1139-keV $\gamma$ ray was placed incorrectly in the $\beta$-decay work of Ref. [4], the reported intensities remain valid and provide a third, independent determination of the $B(E2)$ ratios. As can be seen from Table I, the three data sets provide consistent results; the weighted averages, given
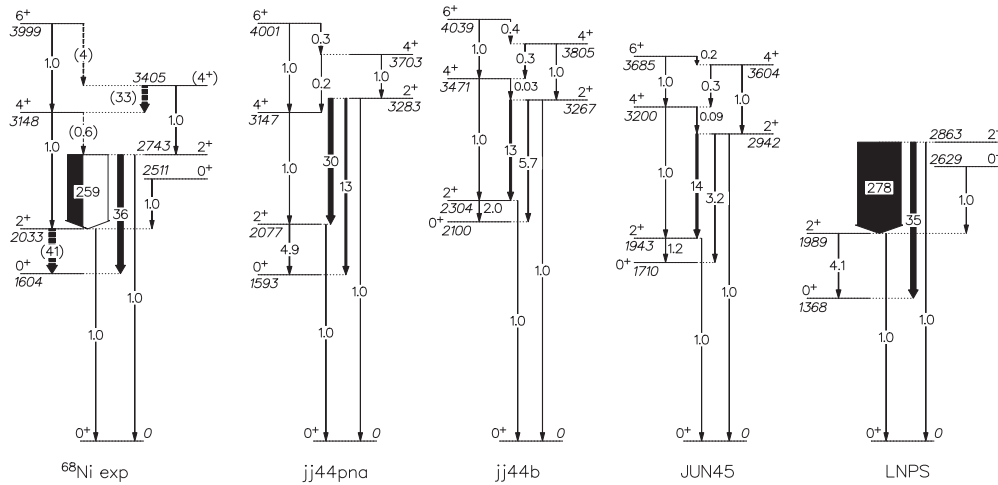
FIG. 4. Decay scheme of $^{68}$Ni deduced from the data ($^{68}$Ni exp) and calculated with the SM using four different interactions (jj44pna, jj44b, and JUN45 in this work and LNPS from Ref. [31]). Arrow widths are proportional to the relative $B(E2)$ strengths, normalized to each level, and are correspondingly labeled. Values in parentheses and with dashed arrows represent upper limits. For the experimental decay scheme, the full arrow width and label for the $2_2^+ \rightarrow 2_1^+$ transition are for the relative $B(E2)$ quoted in Table I, while the black part corresponds to this value reduced by its lower error bar.

in Table I and Fig. 4, can be compared with shell-model calculations, as described below.

The $2_2^+$ state is the only one in $^{68}$Ni for which the intensities of multiple $E2$ decay branches have been established thus far. Upper limits can be placed for some unobserved branches, however, by determining the maximum intensity of the transition that would be indistinguishable from background in the data. A 232-keV, $2_2^+ \rightarrow 0_3^+$ transition was not observed; the two-standard-deviation ($2\sigma$) upper limit on its intensity is 16% that of the 2743-keV branch. Unfortunately, factoring in the $E_\gamma^5$ dependence for the $B(E2)$ ratio yields a rather large upper limit of $R(232) < 4 \times 10^4$ (not indicated in Fig. 4 due to the lack of sensitivity). The possible existence of a 429-keV, $2_1^+ \rightarrow 0_2^+$ transition was investigated as well from coincidence spectra either double gated on the prompt 662- and 710-keV $\gamma$ rays or on a single, delayed 814-keV line in the DIS data. This resulted in a $2\sigma$ upper limit on the intensity of 1.7% relative to the 2033-keV branch to the ground state, and a corresponding ratio $B(E2; 429, 2_1^+ \rightarrow 0_2^+)/B(E2; 2033, 2_1^+ \rightarrow 0_1^+) < 41$. Values for the unobserved 404-keV, $4_1^+ \rightarrow 2_2^+$ and 594-keV, $6_1^+ \rightarrow 4_2^+$ transitions were also extracted; their limits relative to the observed decays from each state are indicated in Fig. 4.

Of the two observed $2_2^+ \rightarrow 0^+$ decay paths, the $E2$ branch to the $0_2^+$ isomer is found to be 36 times stronger than the transition to the ground state [$R(1139)$ in Table I]. This suggests that the $2_2^+$ level is more closely related, in terms of its configuration, to the $0_2^+$ state than to the $0_1^+$ level. Despite the large uncertainty associated with the 710-keV $2_2^+ \rightarrow 2_1^+$ transition (originating from the multipole mixing ratio), it clearly carries significantly more $E2$ strength than the decays to either $0^+$ state, by one or two orders of magnitude (Table I and Fig. 4). Such preferential decay between the $2^+$ states is the result of an admixture between the two underlying configurations.

Shell-model (SM) calculations including only neutron configurations in the $f_{5/2}pg_{9/2}$ valence space were performed with the NuShellX code [27] using a $^{56}$Ni core and the jj44pna [28], jj44b [29], and JUN45 [30] effective interactions for comparison with these data. The results of the calculations are presented in Fig. 4. The jj44pna calculation reproduces the excitation energies of the $0_2^+, 2_1^+, 4_1^+$, and $6_1^+$ states rather well, whereas the energies of the $2_2^+$ and $4_2^+$ states are overpredicted by about 0.5 and 0.3 MeV, respectively. The jj44b and JUN45 calculations deviate more from the data but, overall, are also in reasonable agreement. Although absolute $B(E2)$ strengths were calculated, only the relative values for each level are given for direct comparison with the data.

With all three interactions, the calculations predict the $2_2^+ \rightarrow 0_2^+$ $E2$ transition to be at least several times stronger than the $2_2^+ \rightarrow 0_1^+$ branch, with the $E2$ component of the $2_2^+ \rightarrow 2_1^+$ decay being yet another several times stronger than that. The relative order of these $B(E2)$ strengths matches that of the data, but the scale for the experimental values is larger. The $2_2^+ \rightarrow 0_1^+$ $B(E2)$ value is relatively small in all of the models, and a slight mixture of the wave functions for the lowest two $2^+$ or $0^+$ states can make it arbitrarily smaller. For example, with the jj44pna interaction, a 0.4% admixture of the $2_1^+$ configuration into that of the $2_2^+$ state is sufficient to reproduce the experimental $B(E2)$ ratio $R(1139) = 36(2)$ for the transitions to the $0_2^+$ and $0_1^+$ states. This same adjustment also increases the relative $2_2^+ \rightarrow 2_1^+$ $B(E2)$ strength to about 180 times that of the $2_2^+ \rightarrow 0_1^+$ decay, in agreement with the data. The additional interaction strength required to mix these two levels is only 72 keV, well within the uncertainty of any of these effective Hamiltonians. The main conclusion of this comparison is that the $B(E2; 2_2^+ \rightarrow 0_2^+)$ probability is relatively large in both experiment and theory. Excited-state lifetimes are needed to make more detailed comparisons to theory.

For the decay of the $2_1^+$ level, the large upper limit for the ratio of $B(E2)$ strengths for the unobserved 429-keV and the 2033-keV $\gamma$ rays makes it unclear experimentally which is the preferred branch. The calculations favor the $2_1^+ \rightarrow 0_2^+$ branch over the $2_1^+ \rightarrow 0_1^+$ one by varying degrees, depending on the interaction. However, compared to the $2_2^+$ decay, all three calculations indicate that the $B(E2; 2_1^+ \rightarrow 0_2^+)$ probability is significantly larger than the $B(E2; 2_2^+ \rightarrow 0_2^+)$ strength. (The fact that the former is calculated to be 20 to 50 times larger is obscured in Fig. 4 because the $B(E2)$ ratios are normalized separately for the $2_1^+$ and $2_2^+$ levels.) This observation suggests that the $2_1^+$ and $0_2^+$ levels have similar underlying structure, as also proposed in Refs. [10,31].

The theoretical wave functions are highly mixed in terms of their $\nu[(f_{5/2}, p)_{J_{fp}}^{12-m}(g_{9/2})_{J_g}^m]_J$ configurations involving excitations of $m$ neutrons across the $N = 40$ shell gap. Theory predicts that the ground state is highly paired with components of $\sim$30–45% each in $m = 0$ and 2 configurations, with the remainder having $m \geqslant 4$. The $0_2^+$ state is dominated by $m = 2$ ($J_g = 0$) components. The $2_1^+$ state cannot have $m = 0$ and has about equally large $m = 2$ ($J_g = 2$) and $m = 4$ components. Thus, the theoretical configurations for the $0_2^+$ and $2_1^+$ states are dominated by a $(g_{9/2})^2$ ($J = J_g$) band structure, but there is considerable mixing with states having a $(g_{9/2})^4$ component. In this closed-shell picture, there is a two-particle, two-hole (2p-2h), $2^+$ state, predicted to have $J_g = 0$ and $J_{fp} = 2$, which would correspond to the 2h, $2^+$ level in $^{66}$Ni. With the experimental energy of 1.42 MeV for this excited state in $^{66}$Ni and 1.60 MeV for the energy of the 2p-2h, $0_2^+$ state in $^{68}$Ni, this simple model would predict 3.02 MeV for the $2_2^+$ level in $^{68}$Ni. The actual theoretical wave functions are more complex than this, but the theoretical $2_2^+$ state is still dominated by $J_{fp} = 2$.

The $0_3^+$ level measured at 2511 keV is much lower than the predicted energy, around 3.5 MeV in the $\nu f_{5/2}pg_{9/2}$ model space. Comparison with the MCSM calculations performed in Ref. [10] suggests that it is dominated by 2p-2h proton excitations. There will be a low-lying $2^+$ level associated with a band built on these proton excitations. Such configurations can be described with the LNPS effective interaction [32]. The LNPS calculations of Ref. [31] also predict a very similar energy difference (234 keV) between the $2_2^+$ and $0_3^+$ levels compared to the data and the $B(E2)$ ratios for deexcitations of the $2_2^+$ state are in good agreement with the experimental findings (see Fig. 4). The $2_2^+ \rightarrow 0_3^+$ transition is highly collective, with $B(E2) = 757~e^2\text{fm}^4$ and a ratio of $2.4 \times 10^3$ relative to the $2_2^+ \rightarrow 0_1^+$ branch, but the $E_\gamma^5$ dependence dominates the decay intensity for the 2743-keV transition to the ground state by orders of magnitude. The nonobservation of the 232-keV, $2_2^+ \rightarrow 0_3^+$ transition within the limits established in this work is consistent with the LNPS model.

Both sets of calculations described above predict a $2^+$ level near 3 MeV, arising from neutron configurations in one or proton excitations in the other. In either case, the decay schemes are consistent with the experiment (following a small correction, in the former case). Experimentally, one should find both of these $2^+$ states and determine their lifetimes for a more complete comparison with theory.

In addition to the $2_1^+$ level, limits on the $B(E2)$ ratios for deexcitations of the $4_{1,2}^+$ and $6_1^+$ states were also obtained. Comparing to the predicted values in Fig. 4, it is clear that more than an order of magnitude greater sensitivity would be required for the experimental $B(E2)$ ratios to suitably challenge theory.

In summary, $B(E2)$ ratios were deduced for decays from excited states in $^{68}$Ni populated in DIS and 2nKO reactions, and the energy of the $0_2^+$ isomer at 1603.5(3) keV was confirmed. Comparisons with SM calculations reveal the importance of mixing to account for the observed decay patterns. The $2_1^+$ and $0_2^+$ states appear to have similar structure, and the $2_2^+$ and $0_3^+$ states may as well. Thus, the present data appear to support the shape-coexistence picture of Refs. [10,13]. Absolute strengths of the $2_1^+$ and $2_2^+$ decays are needed to further test the theoretical predictions and quantify the degree of mixing.

---

[1] Kris Heyde and John L. Wood, Rev. Mod. Phys. **83**, 1467 (2011).

[2] M. Bernas *et al.*, Phys. Lett. B **113**, 279 (1982).

[3] R. Broda *et al.*, Phys. Rev. Lett. **74**, 868 (1995).

[4] W. F. Mueller *et al.*, Phys. Rev. C **61**, 054308 (2000).

[5] C. J. Chiara *et al.*, Phys. Rev. C **86**, 041304(R) (2012).

[6] O. Sorlin *et al.*, Phys. Rev. Lett. **88**, 092501 (2002).

[7] M. Girod, Ph. Dessagne, M. Bernas, M. Langevin, F. Pougheon, and P. Roussel, Phys. Rev. C **37**, 2600 (1988).

[8] S. Zhu *et al.*, Phys. Rev. C **85**, 034336 (2012).

[9] R. Broda *et al.*, Phys. Rev. C **86**, 064312 (2012).

[10] S. Suchyta *et al.* (unpublished).

[11] A. Dijon *et al.*, Phys. Rev. C **85**, 031301(R) (2012).

[12] Noritaka Shimizu, Takashi Abe, Yusuke Tsunoda, Yutaka Utsuno, Tooru Yoshida, Takahiro Mizusaki, Michio Honma, and Takaharu Otsuka, Prog. Theor. Exp. Phys. **2012**, 01A205 (2012).

[13] Y. Tsunoda, T. Otsuka, N. Shimizu, M. Honma, and Y. Utsuno, J. Phys.: Conf. Ser. **445**, 012028 (2013).

[14] M. P. Carpenter, R. V. F. Janssens, and S. Zhu, Phys. Rev. C **87**, 041305 (2013).

[15] E. A. McCutchan, Nucl. Data Sheets **113**, 1735 (2012).

[16] Evaluated Nuclear Structure Data File (ENSDF), http://www.nndc.bnl.gov/ensdf

[17] I. Y. Lee, Nucl. Phys. A **520**, 641c (1990).

[18] D. J. Morrissey, B. M. Sherrill, M. Steiner, A. Stolz, and I. Wiedenhoever, Nucl. Instrum. Methods Phys. Res. B **204**, 90 (2003).

[19] D. Bazin, J. A. Caggiano, B. M. Sherrill, J. Yurkon, and A. Zeller, Nucl. Instrum. Methods Phys. Res. B **204**, 629 (2003).

[20] I. Y. Lee *et al.*, Nucl. Phys. A **746**, 255c (2004).

[21] S. Paschalis *et al.*, Nucl. Instrum. Methods Phys. Res. A **709**, 44 (2013).

[22] K. Meierbachtol, D. Bazin, and D. J. Morrissey, Nucl. Instrum. Methods Phys. Res. A **652**, 668 (2011).

[23] K. Wimmer *et al.* (unpublished).

[24] A. R. Poletti, G. D. Dracoulis, A. P. Byrne, A. E. Stuchbery, B. Fabricius, T. Kibédi, and P. M. Davidson, Nucl. Phys. A **615**, 95 (1997).

[25] A. R. Poletti, G. D. Dracoulis, A. P. Byrne, A. E. Stuchbery, B. Fabricius, T. Kibédi, and P. M. Davidson, Nucl. Phys. A **665**, 318 (2000).

[26] T. Ishii, M. Asai, A. Makishima, I. Hossain, M. Ogawa, J. Hasegawa, M. Matsuda, and S. Ichikawa, Phys. Rev. Lett. **84**, 39 (2000).

[27] B. A. Brown, W. D. M. Rae, E. McDonald, and M. Horoi, NUSHELLX@MSU, http://www.nscl.msu.edu/~brown/resources/resources.html; W. D. M. Rae, NUSHELLX, http://www.garsington.eclipse.co.uk/

[28] A. F. Lisetskiy, B. A. Brown, M. Horoi, and H. Grawe, Phys. Rev. C **70**, 044314 (2004).

[29] See endnote [28] in B. Cheal *et al.*, Phys. Rev. Lett. **104**, 252502 (2010).

[30] M. Honma, T. Otsuka, T. Mizusaki, and M. Hjorth-Jensen, Phys. Rev. C **80**, 064323 (2009).

[31] A. Dijon, Ph.D. thesis, Université de Caen Basse-Normandie, France, 2012. The reported excitation energies have been corrected here as per F. Nowacki (private communication).

[32] S. M. Lenzi, F. Nowacki, A. Poves, and K. Sieja, Phys. Rev. C **82**, 054301 (2010).